Supporting Information

In-situ growth of N-doped bamboo-like carbon nanotubes embedded with FeNi nanoparticles on carbon cloth as self-standing cathode for rechargeable zinc-air battery

Neng-Fei Yu *[,1], Xiaoyan Shu [1], Yuanjiang Yang [1], Honghui Wang [3], Qing-Hong Huang[1], Na Tian [2] Ji-Lei Ye *[,1], and Yuping Wu [1,4]

[1] *School of Energy Science and Engineering, Nanjing Tech University, Nanjing 211816, P. R. China*

[2] *State Key Laboratory of Physical Chemistry of Solid Surfaces, Department of Chemistry, College of Chemistry and Chemical Engineering, Collaborative innovation center of Chemistry for Energy Materials, Xiamen University, Xiamen 361005, P. R. China.*

[3] *Key Laboratory of Estuarine Ecological Security and Environmental Health, Fujian Province University, Xiamen University Tan Kah Kee College, Zhangzhou 363105, P. R. China*

4 Confucius Energy Storage Lab, School of Energy and Environment, Southeast University, Nanjing 211189, P. R. China

* *Corresponding author E-mail: yunf@njtech.edu.cn; yejilei@njtech.edu.cn;*

1. Supplementary Figures and Tables

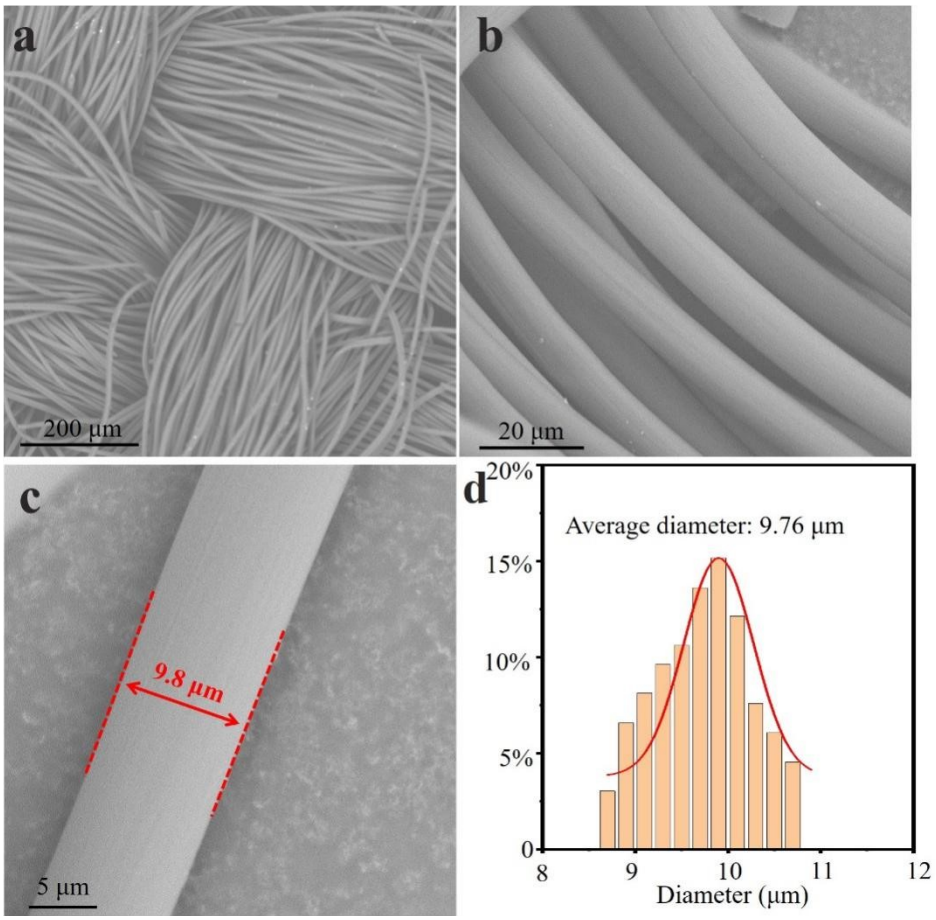

Fig S1. (a-c) SEM images of pristine CC. (d) Diameter distribution of carbon filaments in the CC.

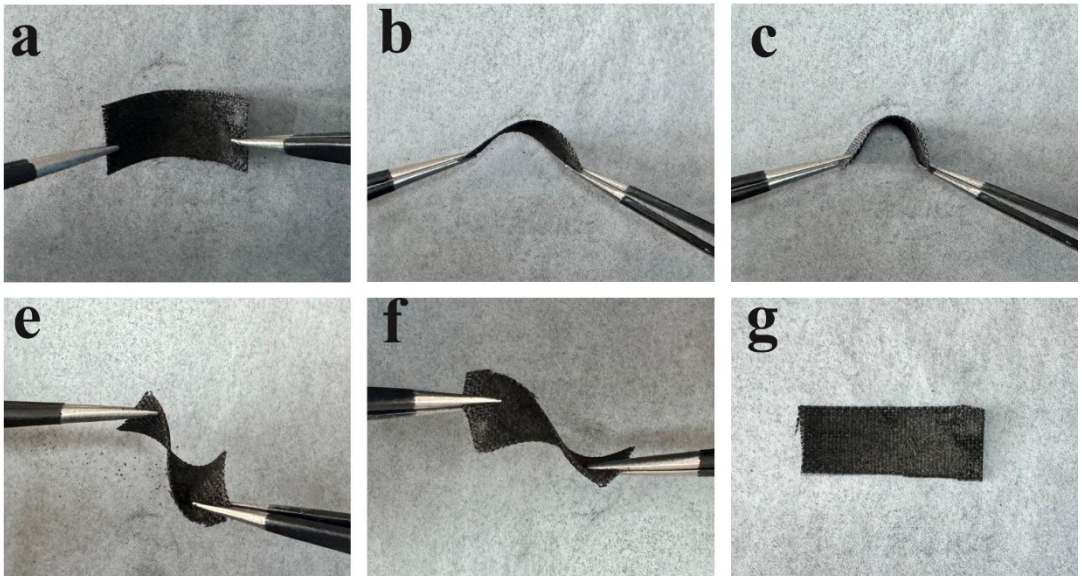

Fig S2. (a-f) Photographs of as-prepared FeNi@NBCNTs/CC under different stress states. (g) Photographs of FeNi@NBCNTs/CC after removing the external stress.

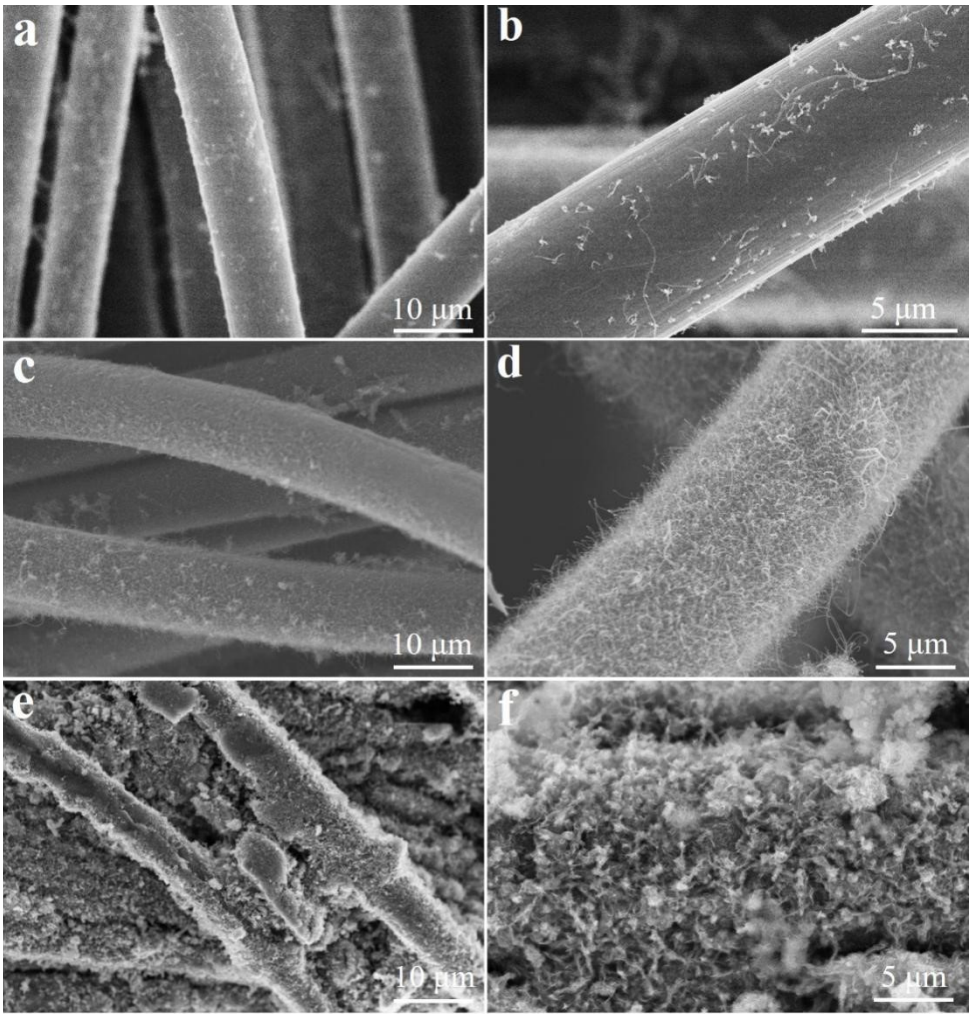

Fig S3. SEM images of FeNi@NBCNTs/CC synthetized at different concentrations of $Fe(NO_3)_3$ and $Ni(NO_3)_2$ in the precursor solution. (a, b) 1 mM $Fe(NO_3)_3$ and 1 mM $Ni(NO_3)_2$. (c, d) 2 mM $Fe(NO_3)_3$ and 2 mM. (e, f) 4 mM $Fe(NO_3)_3$ and 4 mM $Ni(NO_3)_2$.

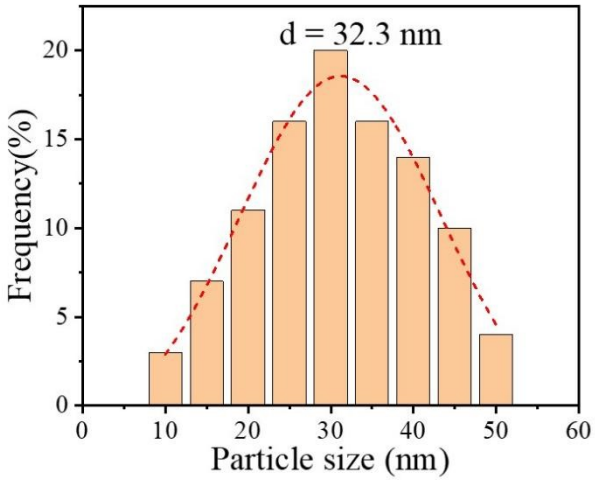

Fig S4. Particle size distribution of FeNi nanoparticles encapsulated within carbon nanotubes

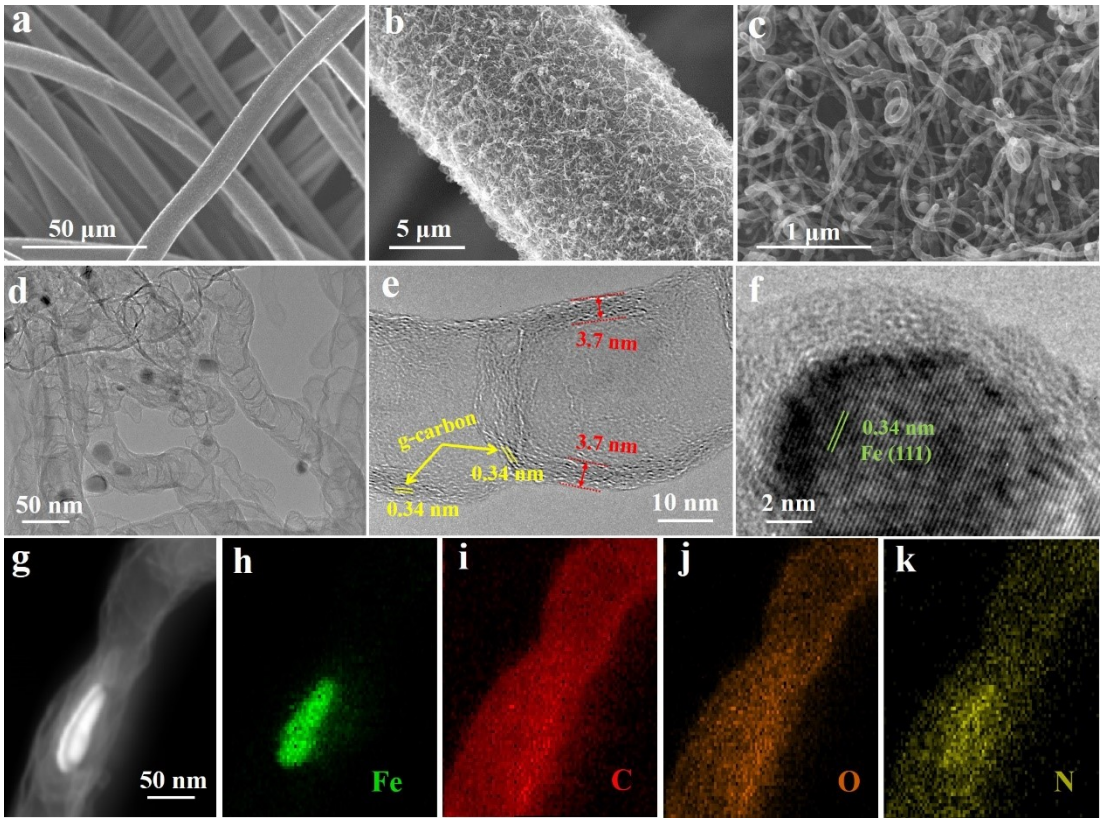

Fig S5. (a-c) SEM images of Fe@NBCNTs/CC. (d) TEM image of Fe@NBCNTs. (e) TEM image for a piece of NBCNTs. (f) TEM image of a Fe nanoparticle. (g-k) HAADF-STEM elemental mapping images of Fe@NBCNTs, showing the presence of Fe, C, N and O elements.

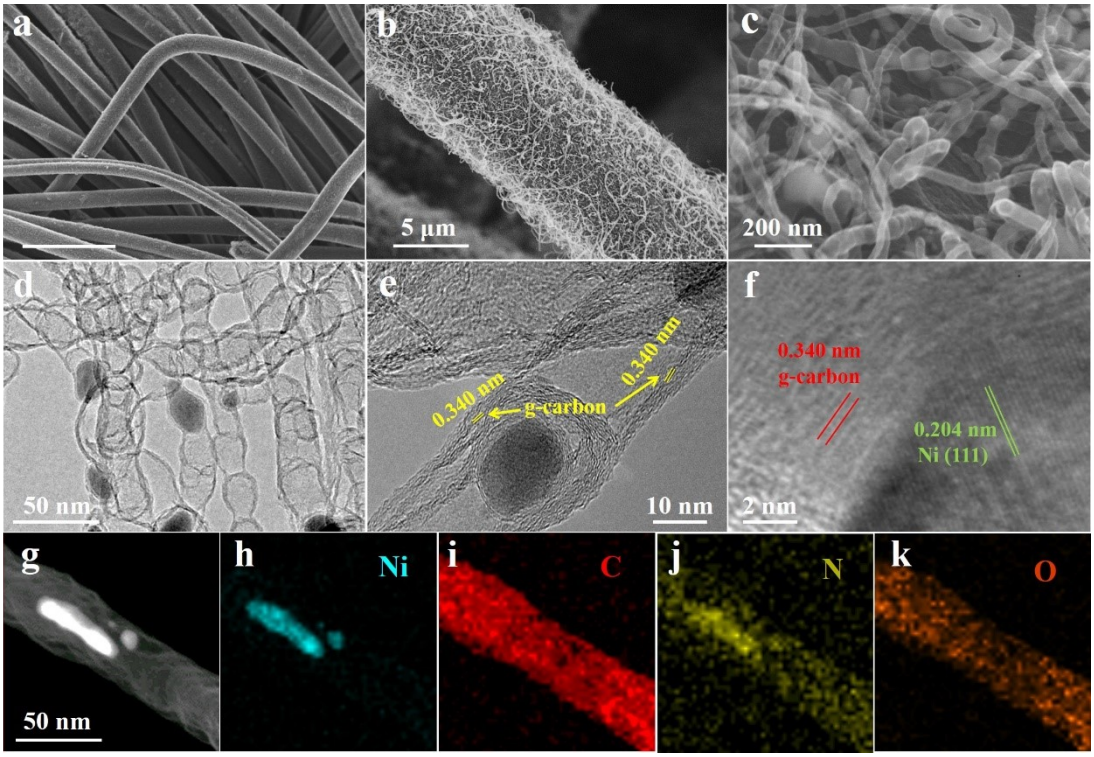

Fig S6. (a-c) SEM images of Ni@NBCNTs/CC. (d) TEM image of Ni@NBCNTs. (e) TEM image for a piece of NBCNTs. (f) TEM image of a Ni nanoparticle. (g-k) HAADF-STEM elemental mapping images of Ni@NBCNTs, showing the presence of Ni, C, N and O elements.

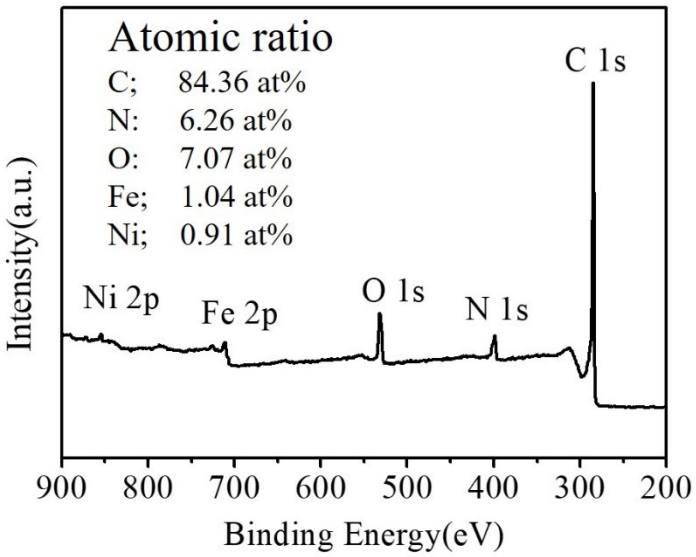

Fig S7. XPS survery spectrum of FeNi@NBCNTs/CC.

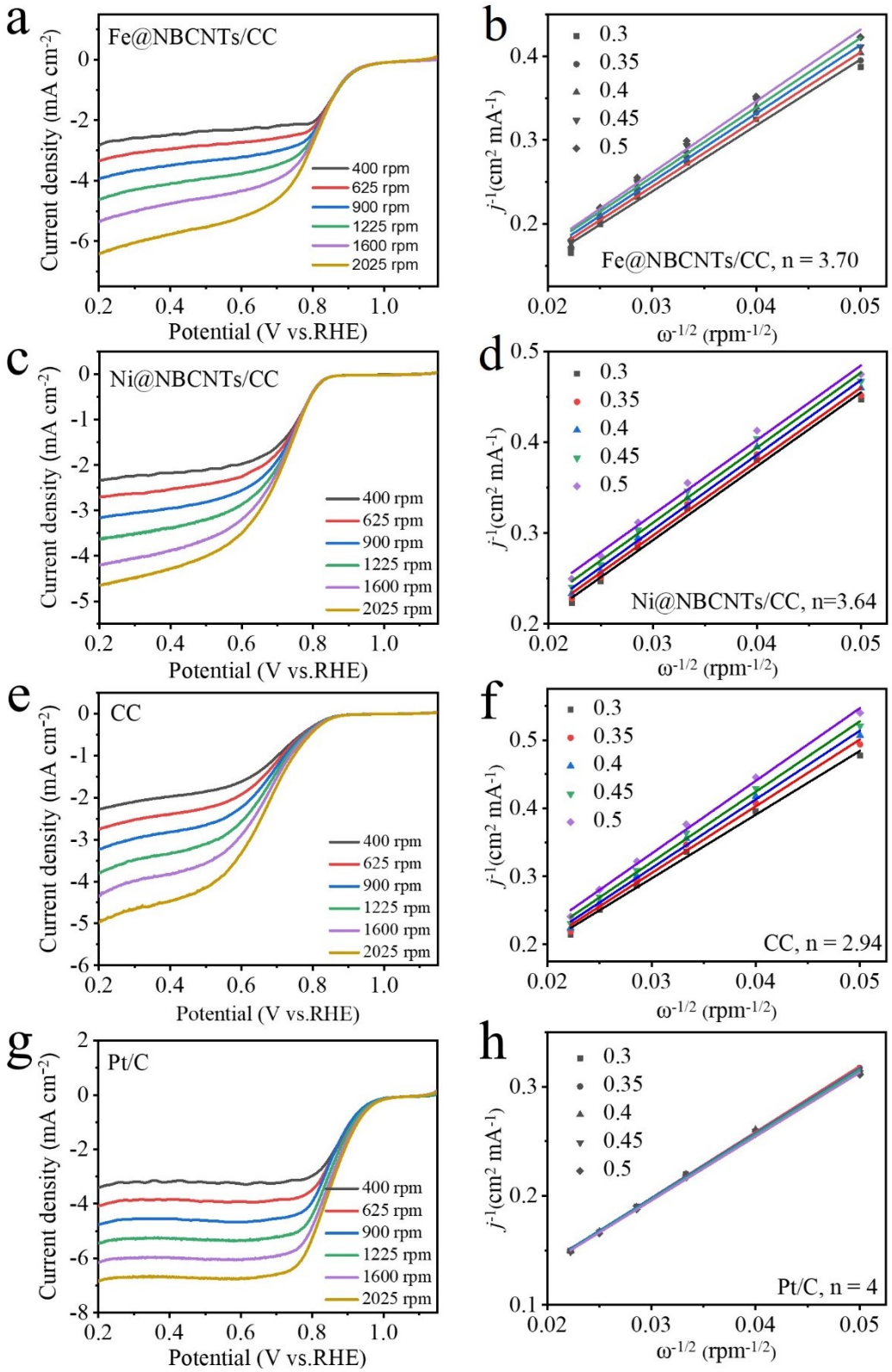

Fig S8. ORR polarization curves (left) at various rotation rates and the corresponding Koutecky-Levich plots (right) obtained at different potentials from (a, b) Fe@NBCNTs/CC, (c, d) Ni@NBCNTs/CC, (e, f) CC and (g, h) Pt/C.

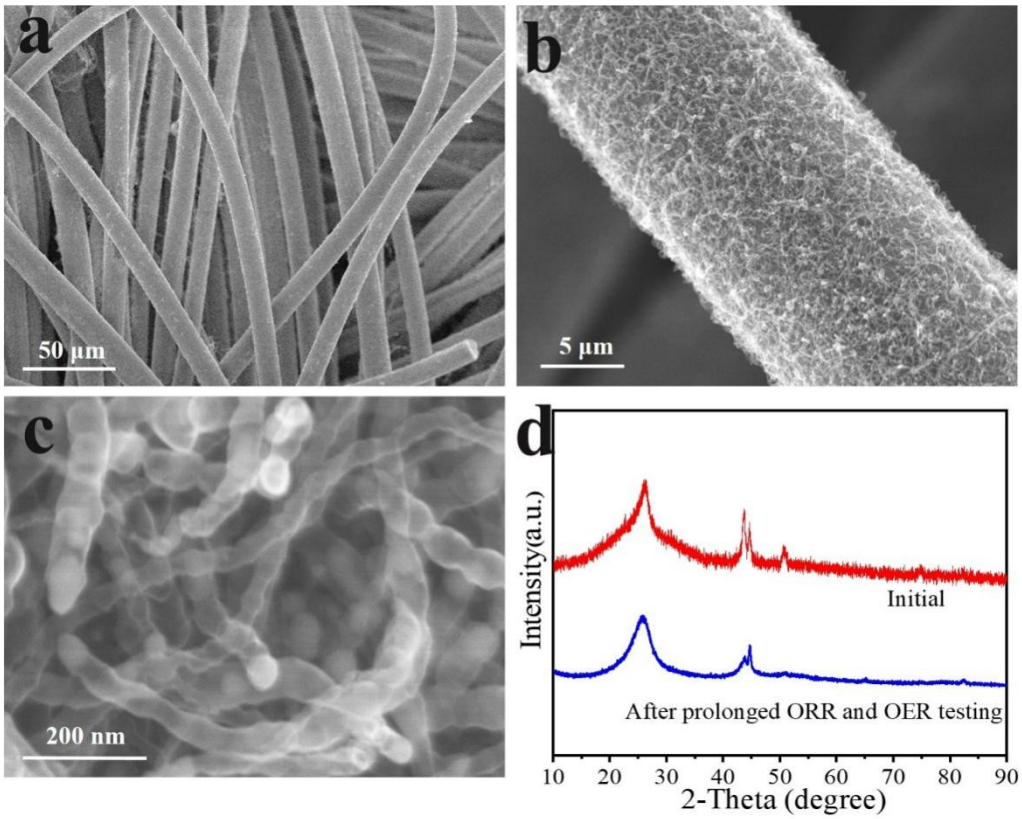

Fig S9. SEM images (a-c) and XRD patterns (d) of FeNi@NBCNTs/CC after long-term ORR and OER stability tests.

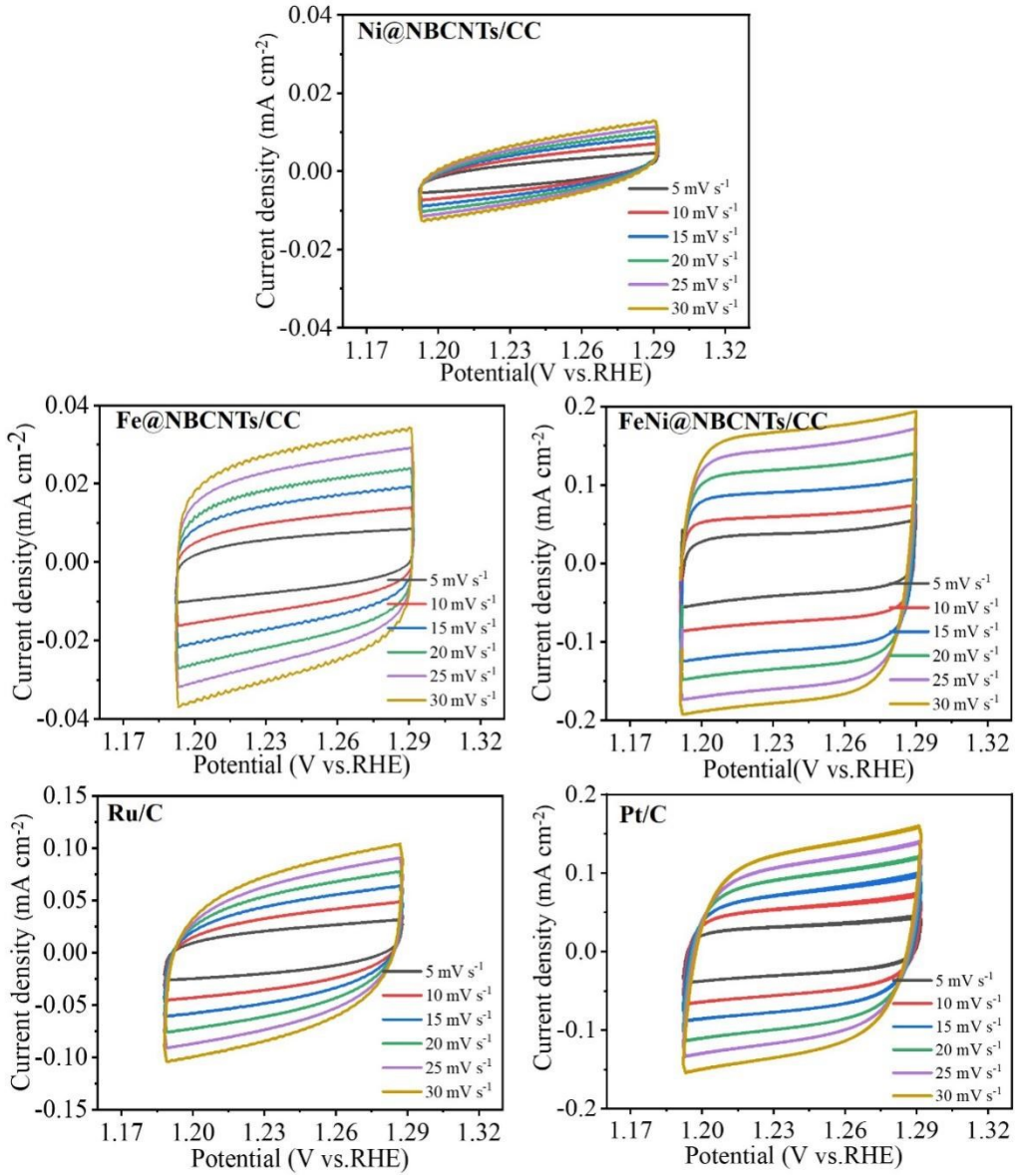

Fig S10. The CV curves recorded at various scan rates ranging from 5 to 30 mV s^{-1}

Fig S11. Photograph of liqiud RZAB of Pt/C+Ru/C cathode with an open-circuit voltage of 1.436 V.

Fig S12. Photograph of flexible RZAB of Pt/C+Ru/C cathode with an open-circuit voltage of 1.343 V.

Table S1. Thorough comparison of performances of recently reported bifunctional oxygen electrocatalysts.

Catalyst	ORR $E_{1/2}$ vs RHE	OER $E_{j=10}$ vs RHE	$\Delta E = (E_{j=10} - E_{1/2})$ vs RHE	Peak power density	Capacity	Stability	Reference
FeNi@NBCNTs/CC	0.90V	1.52V	0.62	171.8mW cm^{-2}	792.6mAhgZn^{-1}	425h@10mA cm^{-2}	This work
CoNC-50	0.84V	1.65V	0.81	125.2mW cm^{-2}	790.8mAhgZn^{-1}	50h@5mA cm^{-2}	[1]
CP-N-C@900	0.86V	1.65V	0.79	279.5mW cm^{-2}	726.3mAhgZn^{-1}	120h@5mA cm^{-2}	[2]
Co-NC+CNT	0.855V	1.695V	0.84	225mW cm^{-2}	906.0mAhgZn^{-1}	200h@5mA cm^{-2}	[3]
P-CoNi@NSCs	0.81V	1.6V	0,79	87.9mW cm^{-2}	745.0mAhgZn^{-1}	430h@10mA cm^{-2}	[4]
Fe_2-N /CNTs-850	0.855V	1.668V	0.814	122.5mW cm^{-2}	764.6mAhgZn^{-1}	160h@3mA cm^{-2}	[5]
$Fe_{12}Ni_{23}Cr_{10}Co_{30}Mn_{25}$/CNT	0.81V	1.514V	0.704	128.6mW cm^{-2}	760mAhgZn^{-1}	256@5mA cm^{-2}	[6]
CMS_2–$NiCo_2O_4$–3	0.82V	1.622V	0.802	175.5mW cm^{-2}	801.1mAhgZn^{-1}	167@5mA cm^{-2}	[7]
Co_9S_8@NiFe-LDH	0.74V	1.62V	0.88	148mW cm^{-2}	780.5mAhgZn^{-1}	200h@10mA cm^{-2}	[8]
FeNi/NS-C	0.83V	1.585V	0.755	144mW cm^{-2}	821.0mAhgZn^{-1}	1000h@5mA cm^{-2}	[9]
Co/N-HPCs-800	0.86V	1.597V	0.737	159.67mW cm^{-2}	787.94mAhgZn^{-1}	30h@5mA cm^{-2}	[10]
Co-NC@Nb-TiOx	0.86V	1.71V	0.85	123.46mW cm^{-2}	780.4mAhgZn^{-1}	225h@5mA cm^{-2}	[11]
CoSx@srGO/CNT	0.81V	1.56V	0.75	66.45mW cm^{-2}	583mAhgZn^{-1}	1000min@10mA cm^{-2}	[12]

MnS/Ni_3S_4	0.83V	1.56V	0,73	158.2mW cm^{-2}	712.3mAhgZn^{-1}	390h@5mA cm^{-2}	[13]
Cox Niy /NC (2:1)	0.85V	1.539V	0.689	143mW cm^{-2}	807mAhgZn^{-1}	100h@10mA cm^{-2}	[14]
FeCo/N–CNTs-800	0.891V	1.61V	0.719	200.4mW cm^{-2}	763.54mAhgZn^{-1}	445h@10mA cm^{-2}	[15]
$NiFe_2O_4$/FeNC	0.83V	1.54V	0.71	140mW cm^{-2}	781.8mAhgZn^{-1}	100h@10mA cm^{-2}	[16]
glu-NiFe	0.85V	1.67V	0.82	127mW cm^{-2}	812.2mAhgZn^{-1}	18h@5mA cm^{-2}	[17]
MC@NC-0.3	0.82V	1.59V	0.77	153mW cm^{-2}	776mAhgZn^{-1}	300h@10mA cm^{-2}	[18]
FeCo-NC@Co2P-NC	0.862V	1.536V	0.674	159.3mW cm^{-2}	881.3mAhgZn^{-1}	140h@10mA cm^{-2}	[19]
CoFe-$Co_{5.47}N$	0.79V	1.634V	0.844	178mW cm^{-2}	709.3mAhgZn^{-1}	1000h@10mA cm^{-2}	[20]

References

[1] Gao Y, Kong D, Cao F, et al. Synergistically tuning the graphitic degree, porosity, and the configuration of active sites for highly active bifunctional catalysts and Zn-air batteries[J]. Nano Research, 2022, 15(9): 7959-7967.

[2] Yu J, Chen Z, Zhong L, et al. Bamboo fiber–derived bifunctional electrocatalyst for rechargeable Zn-air batteries[J]. Ionics, 2023, 29(8): 3193-3202.

[3] Yang H, Yi X, Fan F, et al. Co single atoms building bifunctional catalysts for zinc-air batteries[J]. Materials Letters, 2023, 348.

[4] He X, Fu J, Niu M, et al. Long-range interconnected nanoporous Co/Ni/C composites as bifunctional electrocatalysts for long-life rechargeable zinc-air batteries[J]. Electrochimica Acta, 2022, 413.

[5] Liu R, Wang Y, Zheng W, et al. FeCoP2 Nanoparticles Embedded in a Hybrid Carbon Matrix as a High Performance Bifunctional Catalyst of the Advanced Zinc–Air Battery[J]. Energy & Fuels, 2023, 37(2): 1344-1352.

[6] Cao X, Gao Y, Wang Z, et al. FeNiCrCoMn High-Entropy Alloy Nanoparticles Loaded on Carbon Nanotubes as Bifunctional Oxygen Catalysts for Rechargeable Zinc-Air Batteries[J]. ACS Applied Materials & Interfaces, 2023, 15(27): 32365-32375.

[7] Wang C, Wang T, Liu Q, et al. Starch-based porous carbon microsphere composited NiCo2O4 nanoflower as bifunctional electrocatalyst for zinc-air battery[J]. International Journal of Biological Macromolecules, 2023, 241.

[8] Zhou Y, Si J, Wang H, et al. Co9S8@NiFe-LDH Bifunctional Electrocatalysts as High-

Efficiency Cathodes for Zn–Air Batteries[J]. Energy & Fuels, 2023, 37(13): 9619-9625.
[9] Li X, Liu Y, Wen J, et al. N,S-Codoped Carbon Nanostructures Encapsulated with FeNi Nanoparticles as a Bifunctional Electrocatalyst for Rechargeable Zn–Air Batteries[J]. ACS Applied Nano Materials, 2023, 6(4): 2719-2728.
[10] Nie J, Dong M, Chen G, et al. Biomass-based Hierarchical Porous ORR and OER Bifunctional Catalysts with Strong Stability for Zn-Air Batteries[J]. ACS Sustainable Chemistry & Engineering, 2023, 11(30): 11161-11171.
[11] Wan T, Wang H, Wu L, et al. Niobium-doped conductive TiO-TiO2 heterostructure supported bifunctional catalyst for efficient and stable zinc-air batteries[J]. Journal of Colloid and Interface Science, 2023, 651: 27-35.
[12] Jin Park B, Lee H, Kim J, et al. Hierarchical CoSx/graphene/carbon nanotube hybrid architectures for bifunctional electrocatalysts in zinc-air battery[J]. Journal of Industrial and Engineering Chemistry, 2022, 109: 413-421.
[13] Fan W, Li G. Waxberry-Like MnS/Ni3S4as High-Efficiency Bi-Functional Catalyst for Zn-Air Batteries[J]. Chemistry – A European Journal, 2023, 29(31).
[14] Liu H, Hua D, Wang R, et al. High-performance bifunctional oxygen electrocatalysts for zinc-air batteries over nitrogen-doped carbon encapsulating CoNi nanoparticles[J]. Journal of Physics D: Applied Physics, 2022, 55(48).
[15] Chen J, Zhu J, Li S, et al. In situconstruction of FeCo alloy nanoparticles embedded in nitrogen-doped bamboo-like carbon nanotubes as a bifunctional electrocatalyst for Zn–air batteries[J]. Dalton Transactions, 2022, 51(38): 14498-14507.
[16] Chen Y, Li G, Hong L, et al. FeNC Catalysts Decorated with NiFe2O4 to Enhance Bifunctional Activity for Zn–Air Batteries[J]. ACS Applied Energy Materials, 2023, 6(11): 6357-6369.
[17] Chen X, Chen D, Li G, et al. FeNi incorporated N doped carbon nanotubes from glucosamine hydrochloride as highly efficient bifunctional catalyst for long term rechargeable zinc-air batteries[J]. Electrochimica Acta, 2022, 428.
[18] Peng L, Peng X, Zhu Z, et al. Efficient MnO and Co nanoparticles coated with N-doped carbon as a bifunctional electrocatalyst for rechargeable Zn-air batteries[J]. International Journal of Hydrogen Energy, 2023, 48(50): 19126-19136.
[19] Yu T, Cao X, Song R, et al. MOF-derived FeCo-NC@Co2P-NC as a high-performance bifunctional electrocatalyst for rechargeable Zn-Air batteries[J]. Journal of Alloys and Compounds, 2023, 939.
[20] Zhang J, Liu J, Liu B, et al. CoFe-CoxN heterojunction encapsulated by lignin-derived nitrogen-doped biochar as bifunctional oxygen electrocatalysts for zinc-air batteries[J]. Chemical Engineering Science, 2023, 280.